Mathematics

https://www.aimspress.com/journal/Math

AIMS Mathematics, 11(8): 26006–26025.
DOI: 10.3934/math.20261042
Received: 21 June 2026
Revised: 31 July 2026
Accepted: 17 August 2026
Published: 20 August 2026

Research article

A globally convergent inertial-relaxed hybrid CGPM for constrained nonlinear equations with its applications

Dandan Li[1], **Songhua Wang**[2], **and Jiaqi Wu**[3,*]

[1] School of Artificial Intelligence, Guangzhou Huashang College, Guangzhou 511300, China
[2] School of Mathematics, Physics and Statistics, Baise University, Baise 533099, China
[3] School of Computer Science, Guangdong University of Finance, Guangzhou 510521, China

* **Correspondence:** Email: wjqeasy@163.com.

Abstract: This paper presents a globally convergent inertial-relaxed hybrid conjugate gradient projection (IRHCGP) method for solving constrained nonlinear equations. The proposed method integrates an inertial-relaxed extrapolation strategy into a hybrid conjugate gradient projection framework. A new hybrid conjugate parameter is constructed to generate an effective search direction, which is proved to satisfy both the sufficient descent condition and a trust-region-type bound. These properties provide the theoretical foundation for establishing the global convergence of the proposed method under mild assumptions. Extensive numerical experiments are conducted on large-scale constrained nonlinear equations with various dimensions and initial points, and the proposed method is further applied to impulse noise image restoration. The results demonstrate that the proposed method is competitive and superior to several existing methods in terms of running time, number of function evaluations, and number of iterations.

Keywords: nonlinear equations; inertial-relaxed technique; sufficient descent; global convergence; impulse noise image restoration
Mathematics Subject Classification: 65K05, 90C30, 90C56, 90C90

1. Introduction

1.1. Background and problem

Nonlinear equations play a crucial role in various real-world applications, including split feasibility problems, compressive sensing, machine learning, and electrical power systems (e.g., [1–4]). Moreover, problems involving Bregman distances and variational inequalities can often be reformulated as nonlinear equations, thereby extending their applicability to a wider range of optimization and equilibrium models (e.g., [5, 6]). Recent advances in iterative solution methods, particularly in areas such as image denoising (e.g., [7]) and discretized nonlinear partial differential equations (e.g., [8]), have demonstrated the effectiveness of these techniques in high-dimensional settings. Motivated by these broad applications, this paper focuses on systems of constrained nonlinear equations, which are expressed as follows:

$$F(x) = 0, \quad x \in C, \tag{1.1}$$

where $F : R^n \to R^n$ is a monotone and continuous mapping, and C is a nonempty, closed, and convex set. The monotonicity of the mapping F guarantees that the inequality $(F(x) - F(y))^T(x - y) \geq 0$ holds for any $x, y \in R^n$. For simplicity, we assume throughout this paper that the solution set C_* of problem (1.1) is nonempty.

1.2. Related works

Over the past few decades, various numerical methods have been developed to solve systems of nonlinear equations, with many of these methods benefiting from the projection technique. These methods can generally be classified into two categories: Jacobian-based projection methods and Jacobian-free projection methods. The first category includes Newton-type projection methods (e.g., [9, 10]) and trust region-type projection methods (e.g., [11, 12]). While these Jacobian-based projection methods exhibit rapid convergence rates, they often require the computation and storage of the Jacobian matrix (or its approximation) value during their iterative process. This can make them inefficient and time-consuming for solving large-scale nonlinear equations. In contrast, the second category consists of spectral gradient projection methods, CGPMs, and spectral CGPMs. These methods have garnered significant attention due to their Jacobian-free features. Representative developments in this category include the following. Li et al. [13] proposed a projection-based hybrid spectral gradient method for nonlinear equations with convex constraints, which utilizes a convex combination technique to design a novel spectral parameter inspired by classical spectral gradient methods. Extending this direction, Li et al. [14] presented a projection-based spectral conjugate gradient method for constrained nonlinear equations, which incorporates two bounded spectral parameters through the quasi-Newton condition and double-truncating technique. Progress has also been made in conjugate gradient-based formulations. For instance, Liu et al. [15] later introduced three scaled three-term conjugate gradient methods that extend to solve nonlinear equations, offering the advantages of low storage and the use of only function values. Similarly, Kumam et al. [16] modified the conjugate gradient parameter proposed by Zhu et al. [17] and extended it to solve large-scale systems of nonlinear equations. From a theoretical perspective, Ou et al. [18] developed a general framework that provides a unified convergence analysis of the derivative-free projection-based method for solving large-scale constrained nonlinear monotone equations. Jiang et al. [19] developed an improved memoryless Broyden-Fletcher-Goldfarb-Shanno (BFGS) search direction by incorporating a novel truncation scheme and a restart procedure, and designed a new self-adjusting line search criterion.

In recent years, there has been increasing interest in the inertial-relaxed technique, which is originally developed in [20] for solving nonlinear equations. This technique, stemming from the classical "heavy ball" method, plays a crucial role in accelerating convergence speed [21, 22]. Several researchers have incorporated this technique into the framework of CGPMs. For instance, Aij et al. [23] proposed a derivative-free method that integrates an inertial step to enhance convergence. Building on this momentum, Liu et al. [24] introduced an inertial-type CGPM that incorporates a restart procedure, which involves a new two-term composite restart direction with a flexible non-zero vector and a tuning parameter. Further developments include refined search directions and hybrid formulations. Zheng et al. [25] enhanced the Fletcher-Reeves (FR) conjugate parameter using a shrinkage multiplier, which leads to a derivative-free two-term search direction and its extended spectral version. Similarly, Liu et al. [26] proposed an accelerated spectral conjugate gradient-type projection method to solve nonlinear monotone equations, which utilizes three-step successive information to generate inertial iterates and incorporates a composite search direction framework with an effective restart strategy. Zhuo et al. [27] also contributed an inertial three-term hybrid CGPM, combining inertial extrapolation with hyperplance projection to handle nonlinear pseudo-monotone equations with convex constraints.

Inspired by these recent advancements, as well as the classical works [28–30], we propose an inertial-relaxed hybrid conjugate gradient projection (IRHCGP) method for solving constrained nonlinear equations. This method integrates the advantages of the inertial-relaxed technique and the conjugate gradient projection framework. To further elaborate on the proposed method, the structure of this paper is organized as follows. Section 2 presents the motivation and detailed description of the proposed method. Section 3 establishes the global convergence of the proposed method. Sections 4 and 5 provide comprehensive experimental results, including large-scale nonlinear equations and applications on impulse noise image restoration. Finally, Section 6 concludes the paper with a summary of the findings.

2. Motivation and method description

In this section, we begin by reviewing one of the most effective methods for solving the minimization problem $\min_{x\in R^n} f(x)$, where $f : R^n \to R^n$ is a continuously differentiable function. This method is known as the conjugate gradient method, which relies on a step-length determined by a suitable line search and the search direction defined by an effective conjugate parameter. The commonly used conjugate parameters are as follows:

$$\beta_k^{FR} = \frac{\|g(x_k)\|^2}{\|g(x_{k-1})\|^2}, \quad \beta_k^{HS} = \frac{g(x_k)^T w_{k-1}}{d_{k-1}^T w_{k-1}}, \quad \beta_k^{PRP} = \frac{g(x_k)^T w_{k-1}}{\|g_{k-1}\|^2},$$

$$\beta_k^{DY} = \frac{\|g(x_k)\|^2}{d_{k-1}^T w_{k-1}}, \quad \beta_k^{LS} = \frac{g(x_k)^T w_{k-1}}{-g_{k-1}^T d_{k-1}}, \quad \beta_k^{CD} = \frac{\|g(x_k)\|^2}{-g_{k-1}^T d_{k-1}},$$

where $g(x_k) := \nabla f(x_k)$ and $w_{k-1} = g(x_k) - g(x_{k-1})$. In recent advancements, Andrei [28] introduced a hybrid conjugate gradient method that combines the Dai-Yuan (DY) and Hestenes-Stiefel (HS) methods by using a convex combination. Specifically, the conjugate parameter in this method is defined as

$$\beta_k^A = (1 - \theta_k)\beta_k^{HS} + \theta_k\beta_k^{DY},$$

where $\theta_k \in [0, 1]$ is the hybrid weight coefficient. In a similar vein, Andrei [29] proposed another hybrid conjugate gradient method with the conjugate parameter

$$\beta_k^B = (1 - \theta_k)\beta_k^{PRP} + \theta_k\beta_k^{DY}.$$

Additionally, Wei et al. [30] presented a modified HS-type conjugate gradient method, which introduces the conjugate parameter

$$\beta_k^C = \frac{g(x_k)^T \left(g(x_k) - \frac{g(x_k)^T g(x_{k-1})}{\|g(x_{k-1})\|^2} g(x_{k-1})\right)}{d_{k-1}^T w_{k-1}}.$$

Motivated by the hybrid strategies [28,29], we define a new conjugate gradient parameter by combining the numerator structures of β_k^{FR} and β_k^C in [30]. In addition, we revise their denominator terms in order to obtain a parameter that satisfies both the sufficient descent condition and the trust region condition. Specifically, the new parameter is defined by

$$\begin{aligned} \bar{\beta}_k &= \frac{(1-\theta_k)\|g(x_k)\|^2 + \theta_k \left(\|g(x_k)\|^2 - \frac{\left(g(x_k)^T d_{k-1}\right)^2}{\|d_{k-1}\|^2}\right)}{\max\left\{\bar{\eta}\|g(x_k)\|\|d_{k-1}\|, d_{k-1}^T w_{k-1}, \|g(x_{k-1})\|^2\right\}} \\ &= \frac{\|g(x_k)\|^2 - \theta_k \frac{\left(g(x_k)^T d_{k-1}\right)^2}{\|d_{k-1}\|^2}}{\max\left\{\bar{\eta}\|g(x_k)\|\|d_{k-1}\|, d_{k-1}^T w_{k-1}, \|g(x_{k-1})\|^2\right\}}. \end{aligned}$$

Together with this novel conjugate parameter and the integration of the inertial-relaxed and projection techniques, we propose an IRHCGP method for finding solutions of constrained nonlinear equations. To enhance the convergence speed of the proposed method, we introduce the inertial-relaxed technique, which computes the inertial extrapolation point $y_k = x_k + t_k(x_k - x_{k-1})$. The inertial extrapolation step-length t_k is determined by the following formula:

$$t_k = \begin{cases} \min\left\{t, \frac{1}{k^2\|x_k - x_{k-1}\|^2}\right\}, & \text{if } x_k \neq x_{k-1}, \\ t, & \text{otherwise}, \end{cases} \tag{2.1}$$

where $t \in [0, 1)$. Based on this inertial extrapolation point and the definition of $\bar{\beta}_k$, we extend the conjugate parameter for problem (1.1):

$$\beta_k = \frac{\|F(y_k)\|^2 - \theta_k \frac{\left(F(y_k)^T d_{k-1}\right)^2}{\|d_{k-1}\|^2}}{\max\left\{\eta\|F(y_k)\|\|d_{k-1}\|, d_{k-1}^T v_{k-1}, \|F(y_{k-1})\|^2\right\}}, \tag{2.2}$$

where $v_{k-1} = F(y_k) - F(y_{k-1})$. The condition $\eta > 1$ is imposed to guarantee the sufficient property of the generated direction. Nevertheless, a large value of η may enlarge the denominator of β_k, thereby reducing the contribution of the previous direction d_{k-1} and weakening the hybrid conjugate-gradient feature. Therefore, in practical implementations, η should be selected moderately to balance theoretical stability and numerical efficiency. Following the choice commonly adopted in related studies, we set the hybrid weight coefficient as $\theta_k = |F(y_k)^T F(y_{k-1})|/(\|F(y_k)\|\|F(y_{k-1})\|)$. The search direction is then defined as

$$d_0 = -F(y_0), \quad d_k = -F(y_k) + \beta_k d_{k-1}, \quad \forall k \geq 1. \tag{2.3}$$

To determine the trial point, we use an adaptive line search strategy [31] to generate the trial point $z_k = y_k + \alpha_k d_k$ with the step-length $\alpha_k = r^{m_k}$ and $r \in (0, 1)$. Here, m_k is the smallest integer that satisfies

$$-F(y_k + r^{m_k} d_k)^T d_k \geq \tau r^{m_k} \Phi(m_k)\|d_k\|^2, \tag{2.4}$$

where $\tau \in (0,1)$ and $\Phi(m_k) = \max\{\phi_1, \min\{\phi_2, \|F(y_k + r^{m_k} d_k)\|^2\}\}$ with $\phi_2 > \phi_1 > 0$. For constraint handling, we introduce the projection technique to check if the trial point falls within the constraint set. The projection operator T_C for a closed convex set C is defined as

$$T_C[x] = \arg\min\{\|x - y\| \mid y \in C\}, \quad \forall x \in R^n,$$

and satisfies the well-known non-expansive property

$$\|T_C[x] - T_C[y]\| \le \|x - y\|, \quad \forall x, y \in R^n. \tag{2.5}$$

Thus, the next iterative point is updated by the following projection rule

$$x_{k+1} = T_C\left[y_k - \kappa\pi_k F(z_k)\right], \tag{2.6}$$

where $\pi_k = F(z_k)^T(y_k - z_k)/\|F(z_k)\|^2$ and $\kappa \in (0,2)$.

Incorporating all these techniques, we present the complete procedure for the IRHCGP method for problem (1.1). The detailed steps are outlined in Algorithm 1.

Algorithm 1

Step 0. Initialize $x_0 := x_{-1} \in R^n$ and select the parameters: Tol $\in (0,1)$, $t \in [0,1)$, $\eta > 1$, $\tau, r \in (0,1)$, $0 < \phi_1 < \phi_2$, $\kappa \in (0,2)$. Set iteration counter $k := 0$.
Step 1. If $\|F(x_k)\| \le$ Tol, stop. Otherwise, compute the inertial extrapolation point $y_k = x_k + t_k(x_k - x_{k-1})$ by (2.1).
Step 2. If $\|F(y_k)\| \le$ Tol, stop. Otherwise, compute the search direction d_k by (2.3) and (2.2).
Step 3. Find the smallest integer $m_k \ge 0$ such that (2.4) holds. Then, set $\alpha_k = r^{m_k}$ and $z_k = y_k + \alpha_k d_k$.
Step 4. If $\|F(z_k)\| \le$ Tol, stop. Otherwise, update the next iterative point by (2.6).
Step 5. Set $k := k + 1$ and return to Step 1.

Remark 1. *From the update rule defined in* (2.1)*, we conclude that* $t_k\|x_k - x_{k-1}\|^2 \le \frac{1}{k^2}$ *for all* $k \ge 0$*, which implies that*

$$\sum_{k=0}^{\infty} t_k\|x_k - x_{k-1}\|^2 < \infty.$$

This further indicates that $\lim_{k\to\infty} t_k\|x_k - x_{k-1}\|^2 = 0$.

3. Global convergence

In this section, we show that the search direction defined in (2.3) satisfies the sufficient descent and trust region conditions, which are crucial for establishing the global convergence of the proposed method. We begin by showing the sufficient descent condition in the following lemma.

Lemma 1. *The sequence* $\{d_k\}$ *generated by the IRHCGP method satisfies the sufficient descent condition, i.e.,*

$$F(y_k)^T d_k \le -a_1\|F(y_k)\|^2$$

with $a_1 = (\eta - 1)/\eta$ *for all* $k \ge 0$.

Proof. It follows from (2.3) that $F(y_0)^T d_0 = -\|F(y_0)\|^2 \le -a_1\|F(y_0)\|^2$ when $k = 0$. For $k \ge 1$, it also follows from (2.2) that

$$|\beta_k| \le \frac{\|F(y_k)\|^2}{\eta\|F(y_k)\|\|d_{k-1}\|} = \frac{\|F(y_k)\|}{\eta\|d_{k-1}\|}. \tag{3.1}$$

Multiplying both sides of (2.3) by $F(y_k)^T$ and substituting (3.1) into the formula, we obtain:

$$F(y_k)^T d_k \le -\|F(y_k)\|^2 + |\beta_k|\,\|F(y_k)\|\|d_{k-1}\| \le -\left(1 - \frac{1}{\eta}\right)\|F(y_k)\|^2.$$

Hence, the result is completed. □

Along with sufficient descent, controlling the magnitude of the search direction is vital for numerical stability and convergence. The next lemma establishes such bounds, linking the norm of the search direction to optimality error.

Lemma 2. *The sequence $\{d_k\}$ generated by the IRHCGP method satisfies the trust region condition, i.e.,*

$$a_1\|F(y_k)\| \le \|d_k\| \le a_2\|F(y_k)\|$$

with $a_2 = (\eta + 1)/\eta$ for all $k \ge 0$.

Proof. Applying the Cauchy-Schwarz inequality and invoking Lemma 1, we obtain

$$-\|F(y_k)\|\|d_k\| \le F(y_k)^T d_k \le -a_1\|F(y_k)\|^2,$$

which yields the lower bound:

$$\|d_k\| \ge a_1\|F(y_k)\|.$$

To establish the upper bound, we again use the Cauchy-Schwarz inequality along with (2.3) and (3.1):

$$\|d_k\| \le \|F(y_k)\| + |\beta_k|\|d_{k-1}\| \le \left(1 + \frac{1}{\eta}\right)\|F(y_k)\|.$$

Hence, the result is completed. □

Remark 2. *The condition* (3.1) *is essentially a step-length control that relates the norm of the search direction $\|d_k\|$ to a measure of optimality error $\|F(y_k)\|$. It can be seen as a concrete realization of the classical trust-region constraint. Specifically, the upper bound $\|d_k\| \le a_2\|F(y_k)\|$ prevents excessively large steps, while the lower bound $\|d_k\| \ge a_1\|F(y_k)\|$ safeguards against steps that are too small. This lower bound helps avoid stagnation near stationary points and thus ensures an acceptable convergence rate.*

With the sufficient descent and trust region properties established, we now turn to analyzing the proximity of iterates to a solution. The following lemma provides such a recursive inequality, incorporating the line search and projection steps specific to the algorithm.

Lemma 3. *If the sequences $\{x_k\}$, $\{y_k\}$, and $\{z_k\}$ are generated by the IRHCGP method, then the following inequality holds for all $k \ge 0$ and any $x_* \in C_*$:*

$$\|x_{k+1} - x_*\|^2 + b_k \le \|y_k - x_*\|^2,$$

where $b_k = \kappa(2 - \kappa)\tau^2\phi_1^2\|y_k - z_k\|^4/\|F(z_k)\|^2$.

Proof. Using the monotonicity of F and the fact that $F(x_*) = 0$, we deduce

$$F(z_k)^T(y_k - x_*) = F(z_k)^T(y_k - z_k) + F(z_k)^T(z_k - x_*) \geq F(z_k)^T(y_k - z_k).$$

Combining this with (2.6) and (2.5), we have

$$\begin{aligned} \|x_{k+1} - x_*\|^2 &= \|T_C\left[y_k - \kappa\pi_k F(z_k)\right] - T_C\left[x_*\right]\|^2 \\ &\leq \|y_k - \kappa\pi_k F(z_k) - x_*\|^2 \\ &= \|y_k - x_*\|^2 - 2\kappa\pi_k F(z_k)^T(y_k - x_*) + \kappa^2\pi_k^2\|F(z_k)\|^2 \\ &\leq \|y_k - x_*\|^2 - 2\kappa\pi_k F(z_k)^T(y_k - z_k) + \kappa^2\pi_k^2\|F(z_k)\|^2. \end{aligned}$$

By the definition of π_k, this leads to

$$\|x_{k+1} - x_*\|^2 \leq \|y_k - x_*\|^2 - \kappa(2-\kappa)\frac{(F(z_k)^T(y_k - z_k))^2}{\|F(z_k)\|^2}. \tag{3.2}$$

Furthermore, using the adaptive line search strategy in (2.4) and the definition of z_k, we obtain

$$F(z_k)^T(y_k - z_k) \geq \tau\phi_1\alpha_k^2\|d_k\|^2 = \tau\phi_1\|y_k - z_k\|^2.$$

Substituting it into (3.2), we also obtain

$$\|x_{k+1} - x_*\|^2 \leq \|y_k - x_*\|^2 - \kappa(2-\kappa)\frac{\tau^2\phi_1^2\|y_k - z_k\|^4}{\|F(z_k)\|^2}.$$

Hence, the result is completed. □

To make the recursive relation from Lemma 3 more amenable to summation and limit analysis, it is useful to express it in terms of the squared distance $c_k = \|x_k - x_*\|^2$. This reformulation allows us to leverage the properties of the inertial extrapolation step-length t_k and eventually establish the convergence of the sequence $\{c_k\}$. The following lemma performs this key transformation.

Lemma 4. *If the sequences $\{x_k\}$, $\{y_k\}$, and $\{z_k\}$ are generated by the IRHCGP method, then the following inequality holds for all $k \geq 0$:*

$$c_{k+1} - c_k + b_k \leq t_k(c_k - c_{k-1}) + e_k,$$

where $c_k = \|x_k - x_*\|^2$ and $e_k = t_k(1 + t_k)\|x_k - x_{k-1}\|^2$.

Proof. From the definition of y_k, we have:

$$y_k - x_* = x_k - x_* + t_k(x_k - x_{k-1}) = (1 + t_k)(x_k - x_*) - t_k(x_{k-1} - x_*),$$

which implies:

$$\|y_k - x_*\|^2 = (1 + t_k)\|x_k - x_*\|^2 - t_k\|x_{k-1} - x_*\|^2 + t_k(1 + t_k)\|x_k - x_{k-1}\|^2.$$

Substituting this expression into the inequality established in Lemma 3, we obtain

$$\|x_{k+1} - x_*\|^2 + b_k \leq (1 + t_k)\|x_k - x_*\|^2 - t_k\|x_{k-1} - x_*\|^2 + t_k(1 + t_k)\|x_k - x_{k-1}\|^2.$$

Hence, the result is completed. □

The inequality in Lemma 4 resembles a recursive estimate common in analysis of the algorithm. By carefully manipulating this inequality, we can prove two fundamental facts: The sequence of $\{c_k\}$ converges, and the auxiliary positive term b_k is summable. The following lemma provides the technical details of this argument.

Lemma 5. *If the sequences $\{x_k\}$, $\{y_k\}$, and $\{z_k\}$ are generated by the IRHCGP method, then the following conclusions hold: (i) $\lim_{k\to\infty} c_k$ exists; (ii) $\sum_{k=1}^{\infty} b_k < \infty$.*

Proof. By the definition of e_k and $t_k \in [0, 1)$, we have $e_k \leq 2t_k\|x_k - x_{k-1}\|^2$. Substituting this into the inequality from Lemma 4, we obtain

$$c_{k+1} - c_k \leq c_{k+1} - c_k + b_k \leq t_k(c_k - c_{k-1}) + 2t_k\|x_k - x_{k-1}\|^2.$$

Define $h_k = c_k - c_{k-1}$ and $l_k = 2t_k\|x_k - x_{k-1}\|^2$, then the inequality becomes

$$h_{k+1} \leq t_k h_k + l_k \leq t_k[h_k]_+ + l_k,$$

where $[h_k]_+ = \max(h_k, 0)$. Using the fact that $t_k \in [0, 1)$, we obtain

$$[h_{k+1}]_+ \leq t[h_k]_+ + l_k \leq t^{k+1}[h_0]_+ + \sum_{i=0}^{k} t^i l_{k-i} = \sum_{i=0}^{k} t^i l_{k-i}.$$

Summing both sides over k, we have

$$\sum_{k=0}^{\infty}[h_{k+1}]_+ \leq \sum_{k=0}^{\infty}\left(\sum_{i=0}^{k} t^i l_{k-i}\right) = \frac{1}{1-t}\sum_{k=1}^{\infty} l_k < \infty.$$

Now, we define an auxiliary sequence $o_k := c_k - \sum_{i=1}^{k}[h_i]_+$. Since $c_k > 0$ and the partial sum of $[h_i]_+$ is bounded, $\{o_k\}$ is bounded below. Moreover, we observe

$$\begin{aligned}
o_{k+1} &= c_{k+1} - [h_{k+1}]_+ - \sum_{i=1}^{k}[h_i]_+ \\
&\leq c_{k+1} - h_{k+1} - \sum_{i=1}^{k}[h_i]_+ \\
&= c_{k+1} - (c_{k+1} - c_k) - \sum_{i=1}^{k}[h_i]_+ \\
&= o_k.
\end{aligned}$$

Hence, $\{o_k\}$ is non-increasing and bounded below, so it converges. Since the sum $\sum_{k=1}^{\infty}[h_{k+1}]_+ < \infty$, we conclude that $\{c_k\}$ is convergent.

We recall from Lemma 4 that:

$$\begin{aligned}
b_k &\leq c_k - c_{k+1} + t_k(c_k - c_{k-1}) + e_k \\
&\leq c_k - c_{k+1} + t_k[h_k]_+ + l_k.
\end{aligned}$$

Similarly, summing over k, we obtain

$$\sum_{k=1}^{\infty} b_k \leq c_0 + t\sum_{k=0}^{\infty}[h_k]_+ + \sum_{k=0}^{\infty} l_k < \infty.$$

Hence, the results are completed. □

The convergence and summability results from Lemma 5 allow us to deduce the boundedness of the generated sequences and the asymptotic behavior of certain key quantities. The next lemma formalizes these observations.

Lemma 6. *If the sequences $\{x_k\}$, $\{y_k\}$, and $\{z_k\}$ are generated by the IRHCGP method, then the following conclusions hold: (i) The sequences $\{x_k\}$ and $\{y_k\}$ are both bounded; (ii)* $\lim_{k\to\infty}\|z_k - y_k\| = \lim_{k\to\infty}\alpha_k\|d_k\| = 0$.

Proof. From the definition of c_k and Lemma 5 (i), it follows that the sequence $\{x_k\}$ is bounded. Next, using the definition of y_k, we compute $\|y_k - x_k\|^2 = \|x_k + t_k(x_k - x_{k-1}) - x_k\|^2 \leq t_k\|x_k - x_{k-1}\|^2$. By Remark 1, we know that $\lim_{k\to\infty} t_k\|x_k - x_{k-1}\|^2 = 0$, which implies that

$$\lim_{k\to\infty}\|y_k - x_k\| = 0. \tag{3.3}$$

Thus, the sequence $\{y_k\}$ is also bounded.

By the boundedness of $\{y_k\}$ and the continuity of F, there exists a constant $a_3 > 0$ such that $\|y_k\| \leq a_3$ and $\|F(y_k)\| \leq a_3$. Then, applying Lemma 2, we obtain $\|d_k\| \leq a_2\|F(y_k)\| \leq a_2a_3$, so $\{d_k\}$ is bounded. Since $z_k = y_k + \alpha_k d_k$ and $\alpha_k \in (0, 1]$, the boundedness of $\{y_k\}$ and $\{d_k\}$ implies that $\{z_k\}$ is also bounded. Consequently, there exists a constant $a_4 > 0$ such that $\|F(z_k)\| \leq a_4$ for all k. Now, considering the definition of b_k and Lemma 5 (ii), we obtain

$$\frac{\kappa(2-\kappa)\tau^2\phi_1^2}{a_4^2}\sum_{k=1}^{\infty}\|y_k - z_k\|^4 \leq \kappa(2-\kappa)\sum_{k=1}^{\infty}\frac{\tau^2\phi_1^2\|y_k - z_k\|^4}{\|F(z_k)\|^2} = \sum_{k=1}^{\infty} b_k < \infty.$$

Thus, we conclude that $\lim_{k\to\infty}\alpha_k\|d_k\| = 0$. Hence, the results are completed. □

With all the preparatory lemmas in place, we can now prove the main convergence theorem.

Theorem 1. *If the sequences $\{x_k\}$, $\{y_k\}$, and $\{z_k\}$ are generated by the IRHCGP method, then these sequences all converge to a same solution of C_*.*

Proof. We divide the proof into two parts.

(i) We first show that

$$\liminf_{k\to\infty}\|F(y_k)\| = 0. \tag{3.4}$$

Assume by contradiction that the above result does not hold. Then, there exists a constant $a_5 > 0$ such that $\|F(y_k)\| \geq a_5$ for all k. Since the sequences $\{y_k\}$ and $\{d_k\}$ are bounded, there exists a convergent subsequence

$$\lim_{i\to\infty}\|y_{k_i}\| = \bar{y}, \quad \lim_{i\to\infty}\|d_{k_i}\| = \bar{d}.$$

By the continuity of F and Lemma 1, we have

$$F(\bar{y})^T\bar{d} \leq -a_1\|F(\bar{y})\|^2 \leq -a_1a_5^2 < 0. \tag{3.5}$$

On the other hand, Lemma 2 implies that $\|d_k\| \geq a_1\|F(y_k)\| \geq a_1 a_5$, and by Lemma 6 (ii), we know that $\lim_{k\to\infty} \alpha_k = 0$. Then, there exists a value $r^{-1}\alpha_k$ such that the adaptive line search strategy does not hold, i.e.,

$$-F(y_k + r^{-1}\alpha_k d_k)^T d_k < \tau r^{-1}\alpha_k \phi_1 \|d_k\|^2.$$

Letting $k := k_i$ and taking limits as $i \to \infty$, we obtain $F(\bar{y})^T \bar{d} \geq 0$, which contradicts (3.5). Thus, the assumption must be false.

(ii) We now prove that all three sequences converge to a same solution. From the boundedness of $\{y_k\}$, the continuity of F, and (3.4), there exists a subsequence such that

$$\lim_{i\to\infty} \|F(y_{k_i})\| = \|F(\bar{y})\| = 0.$$

This indicates that $\bar{y} \in C$. Moreover, from (3.3), we know that $\bar{y}$ is an accumulation point of $\{x_k\}$. There exists an infinite index set $\mathcal{K}$ such that $\lim_{k\in\mathcal{K},k\to\infty} x_k = \bar{y} \in C$. Setting $x_* := \bar{y}$ in Lemma 5 (i), we conclude

$$\lim_{k\to\infty} \|x_k - \bar{y}\| = \lim_{k\in\mathcal{K},k\to\infty} \|x_k - \bar{y}\| = 0,$$

which implies that $\{x_k\}$ converges to $\bar{y} \in C$. Together with (3.3) and $\lim_{k\to\infty} \|z_k - y_k\| = 0$, we deduce that both $\{y_k\}$ and $\{z_k\}$ converge to $\bar{y}$. Hence, the results are completed. □

4. Numerical experiments

In this section, we apply the IRHCGP method to solve large-scale constrained nonlinear equations and compare its performance with four similar methods, namely, the inertial projected Dai-Yuan (IPDY) [32], Jian's hybrid conjugate gradient projection method (JHCGPM) [33], inertial-relaxed three-term conjugate gradient method (IRTTCGPM) [34], and inertial Dai-Liao algorithm (IDLA) [35]. All the methods are written in Matlab 2025a on a 64-bit Lenovo laptop with Intel(R) Core(TM) i9-13900HX CPU (2.20 GHz) 32.0 GB RAM. For a fair comparison, the algorithmic parameters for the IRHCGP method are selected as follows: Tol $\leq 10^{-6}$, $t = 0.015$, $\tau = 10^{-4}$, $r = 0.55$, $\phi_1 = 10^{-3}$, $\phi_2 = 0.8$, and $\kappa = 1.55$. For the IPDY, JHCGPM, IRTTCGPM, and IDLA methods, the algorithmic parameters are taken directly from their respective references. The experiments are conducted on nine benchmark problems, where the dimensions of each problem are chosen from the set $\{5000, 10000, 50000, 100000, 150000\}$. For each problem and each problem dimension, we consider eight different initial points, defined as follows:

$$x_1 = (1, 1, \ldots, 1)^T, x_2 = (\frac{1}{3}, \frac{1}{3^2}, \ldots, \frac{1}{3^n})^T, x_3 = (\frac{n-1}{n}, \frac{n-2}{n}, \ldots, \frac{n-n}{n})^T, x_4 = (\frac{1}{n}, \frac{2}{n}, \ldots, \frac{n}{n})^T,$$

$$x_5 = (1, \frac{1}{2}, \ldots, \frac{1}{n})^T, x_6 = (0, \frac{1}{n}, \ldots, \frac{n-1}{n})^T, x_7 = (\frac{1}{2}, \frac{1}{2^2}, \ldots, \frac{1}{2^n})^T, x_8 = randn(n, 1).$$

The specific formulations for each of these benchmark problems are as follows:

Problem 1. *Set*

$$F_i(x) = e^{x_i} - 1, \quad \text{for i} = 1, 2, \ldots, \text{n},$$

and $C = \mathbb{R}^n_+$.

Problem 2. *Set*

$$\begin{aligned} F_1(x) &= 2x_1 + 0.5h^2(x_1 + h)^3 x_2, \\ F_i(x) &= 2x_i - x_{i-1} + x_{i+1} + 0.5h^2(x_i + ih)^3, \quad \text{for i} = 2, 3, \ldots, \text{n} - 1, \\ F_n(x) &= 2x_n - x_{n-1} + 0.5h^2(x_n + nh)^3, \end{aligned}$$

and $C = \mathbb{R}^n_+,\ h = \frac{1}{n+1}$.

Problem 3. *Set*

$$F_i(x) = 2x_i - \sin(x_i), \quad \text{for i} = 1, 2, \ldots, \text{n},$$

and $C = [-2, +\infty)$.

Problem 4. *Set*

$$F_i(x) = \log(x_i + 1) - \frac{x_i}{n}, \quad \text{for i} = 1, 2, \ldots, \text{n},$$

and $C = [-1, +\infty)$.

Problem 5. *Set*

$$\begin{aligned} F_1(x) &= e^{x_1} - 1, \\ F_i(x) &= e^{x_i} + x_{i-1} - 1, \quad \text{for i} = 2, 3, \ldots, \text{n}, \end{aligned}$$

and $C = \mathbb{R}^n_+$.

Problem 6. *Set*

$$\begin{aligned} F_1(x) &= x_1 - e^{\cos(\frac{x_1 + x_2}{2})}, \\ F_i(x) &= x_i - e^{\cos(\frac{x_{i-1} + x_i + x_{i+1}}{i})}, \quad \text{for i} = 2, 3, \ldots, \text{n} - 1, \\ F_n(x) &= x_n - e^{\cos(\frac{x_{n-1} + x_n}{n})}, \end{aligned}$$

and $C = \mathbb{R}^n_+$.

Problem 7. *Set*

$$F_i(x) = x_i - \sin(|x_i - 1|), \quad \text{for i} = 1, 2, \ldots, \text{n},$$

and $C = \mathbb{R}^n_+$.

Problem 8. *Set*

$$F_i(x) = (e^{x_i})^2 + \frac{3}{2}\sin(2x_i) - 1, \quad \text{for i} = 1, 2, \ldots, \text{n},$$

and $C = \mathbb{R}^n_+$.

Problem 9. *Set*

$$\begin{aligned} F_1(x) &= 2.5x_1 + x_2 - 1, \\ F_i(x) &= x_{i-1} + 2.5x_i + x_{i+1} - 1, \quad \text{for i} = 2, 3, \ldots, \text{n} - 1, \\ F_n(x) &= x_{n-1} + 2.5x_n - 1, \end{aligned}$$

and $C = \{x \in \mathbb{R}^n : x \geq -3\}$.

To examine the influence of the parameter η, we tested the IRHCGP method with $\eta = 1.5$, 2.0, 2.5, 3.5, 5.5, 10.5, and 15.5, hereafter denoted by IRHCGP15, IRHCGP20, IRHCGP25, IRHCGP35, IRHCGP55, IRHCGP105, and IRHCGP155, respectively. To provide a clearer visualization of the performance of the proposed method, we introduce the performance profile, as developed from the work [36], to generate the figures, which compare the methods in terms of the running time in seconds (RunT), the number of function evaluations (NumF), and the number of iterations (NumF). As shown in Figure 1, the IRHCGP method with $\eta = 3.5$ outperforms the variants with $\eta = 5.5, 10.5$, and 15.5. By contrast, the IRHCGP variants with $1 < \eta \leq 3.5$ exhibit comparable performance, indicating that the method is relatively insensitive to the choice of η within this range. Therefore, we set $\eta = 3.5$ in the subsequent numerical experiments. Besides, we compare the IRHCGP method with the IPDY, JHCGPM, IRTTCGPM, and IDLA methods. As shown in Figure 2, the IRHCGP method solves around 42.78% (48.06% and 51.67%) of the best results in terms of RunT (NumF and NumI) in comparison to the IPDY, JHCGPM, IRTTCGPM, and IDLA methods that solve approximately 20.83% (35% and 38.06%), 20% (39.44% and 36.11%), 8.33% (13.61% and 17.22%), and 10.28% (33.33% and 46.67%), respectively. Based on the data from these tables and figures, we conclude that the IRHCGP method significantly outperforms the comparative methods in terms of RunT, NumF, and NumI. This indicates that the proposed method is particularly effective and promising at handling large-scale constrained nonlinear equations.

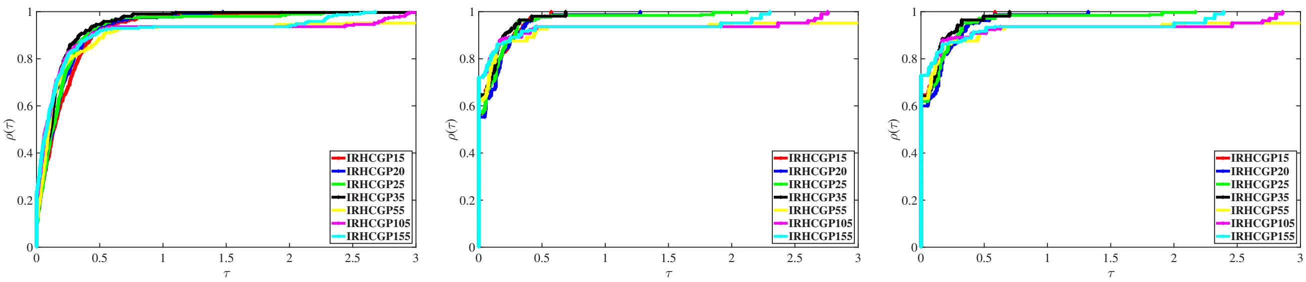

(a) (b) (c)

Figure 1. Comparison of different parameters η: (a) Performance profiles on RunT; (b) Performance profiles on NumF; (c) Performance profiles on NumI.

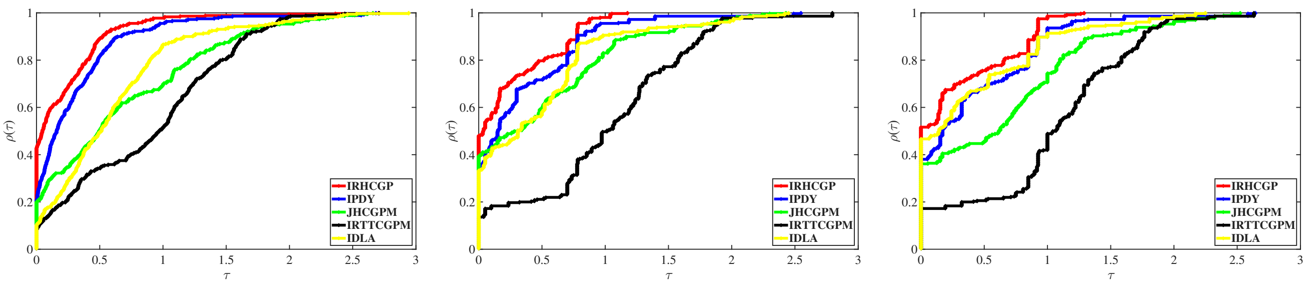

(a) (b) (c)

Figure 2. Comparison of different methods: (a) Performance profiles on RunT; (b) Performance profiles on NumF; (c) Performance profiles on NumI.

5. Applications on impulse noise image restoration

Impulse noise image restoration focuses on reconstructing images that have been significantly degraded due to impulse noise corruption. This restoration typically involves processing large-scale image data and extracting meaningful information from high-dimensional feature spaces. A particularly influential method in this domain is the two-phase approach proposed by Chan et al. [37], which has become a foundational technique for handling impulse noise. This method proceeds in two stages. In the first phase, an adaptive median filter is employed to detect corrupted pixels, which are subsequently marked as the noisy pixel set $\mathcal{N}$. In the second phase, the identified noisy pixels are restored by solving the following smooth unconstrained optimization problem:

$$\min f_\alpha(x) := \sum_{(i,j)\in\mathcal{N}} (2O^1_{i,j} + O^2_{i,j}),$$

where

$$O^1_{i,j} = \sum_{(m,n)\in\mathcal{V}_{i,j}\setminus\mathcal{N}} \varphi_\alpha(x_{i,j} - y_{m,n}), \quad O^2_{i,j} = \sum_{(m,n)\in\mathcal{V}_{i,j}\cap\mathcal{N}} \varphi_\alpha(x_{i,j} - x_{m,n}),$$

and $\mathcal{V}_{i,j}$ denotes the set of four neighboring pixels of the pixel position (i, j). The function $\varphi_\alpha(\cdot)$ represents an edge-preserving potential, designed to retain image structures during restoration. Since f_α is continuously differentiable, the above smooth unconstrained optimization problem can be reformulated through its first-order optimality condition as $F(x) := \nabla f_\alpha(x) = 0$. This nonlinear system is a special case of problem (1.1) with $C = \mathbb{R}^n$, for which the projection operator reduces to the identity mapping. Moreover, as established in [37], when $\varphi_\alpha(\cdot)$ is convex, the gradient mapping $F = \nabla f_\alpha(x)$ is monotone. Therefore, the image restoration problem falls within the nonlinear equation framework considered in this paper.

Experiments are conducted on a benchmark dataset consisting of 24 grayscale images, which are available at https://www.hlevkin.com. These images are artificially corrupted by impulse noise at three different levels: 20%, 40%, and 60%. We assess the performance of three methods: IRHCGP, IPDY, and JHCGPM. For each noise levels, 10 independent trials are performed by using randomly generated noise patterns, and the average results over these trials are reported. The performance metrics include the average number of iterations ($\overline{NumI}$), average running time in seconds ($\overline{RunT}$), and average structural similarity index measure ($\overline{SSIM}$) as summarized in Table 1. A larger $\overline{SSIM}$ value indicates better restoration quality. From the experimental results, the IRHCGP method achieves superior performance, obtaining the best result in 72.22% of the cases for $\overline{NumI}$ and in 70.83% of the cases for $\overline{RunT}$ under the similar $\overline{SSIM}$ values. In contrast, the IPDY and JHCGPM methods obtain only 5.56%(22.22%) and 9.72%(19.44%) of the best results, respectively. These findings clearly demonstrate that the IRHCGP method outperforms the other two methods in both efficiency and promise when restoring images corrupted by impulse noise. Furthermore, the qualitative restoration outcomes are illustrated in Figures 3 and 4, where visual comparisons are shown for 20%, 40%, and 60% noise levels. These images can be successfully restored by these methods.

Table 1. The numerical results for impulse noise image restoration.

Name	Noise	IRHCGP	IPDY	JHCGPM
		$NumI/RunT/SSIM$	$NumI/RunT/SSIM$	$NumI/RunT/SSIM$
airplane	0.2	8.00/0.81/1.00	23.60/2.12/1.00	19.80/2.43/1.00
	0.4	5.00/0.75/0.99	41.00/5.05/0.99	34.00/6.28/0.99
	0.6	59.20/11.02/0.97	50.80/8.42/0.97	46.80/10.35/0.97
airplaneU2	0.2	5.00/2.48/1.00	14.00/6.32/1.00	13.20/6.39/1.00
	0.4	19.60/13.96/0.99	15.20/10.18/0.99	10.00/7.99/0.99
	0.6	27.60/22.08/0.98	23.20/17.01/0.98	23.80/21.62/0.98
brickwall	0.2	8.60/4.01/1.00	19.60/8.31/1.00	15.60/8.09/1.00
	0.4	5.00/3.72/0.99	25.00/15.73/0.99	19.40/15.67/0.99
	0.6	4.00/3.86/0.98	34.80/24.52/0.98	25.80/24.02/0.98
bridge	0.2	9.40/0.91/0.99	20.80/1.84/0.99	16.40/1.78/0.99
	0.4	9.40/1.27/0.97	29.20/3.70/0.97	38.60/6.30/0.97
	0.6	8.00/1.51/0.92	52.40/8.69/0.92	36.80/8.36/0.92
cameraman	0.2	11.40/0.20/0.97	31.20/0.50/0.97	17.20/0.36/0.96
	0.4	7.00/0.22/0.92	39.80/0.99/0.92	76.80/2.70/0.92
	0.6	5.80/0.21/0.86	61.80/1.66/0.86	42.80/1.55/0.85
carpet	0.2	20.00/8.24/1.00	19.00/7.84/1.00	20.40/11.04/1.00
	0.4	22.40/14.03/1.00	35.00/21.92/1.00	10.80/9.41/1.00
	0.6	28.40/20.34/0.99	38.40/27.59/0.99	36.60/36.44/0.99
clown	0.2	8.00/0.78/0.99	26.60/2.30/0.99	18.80/2.26/0.99
	0.4	6.00/0.88/0.99	26.00/3.22/0.99	24.40/4.30/0.99
	0.6	5.00/1.01/0.96	46.60/7.71/0.96	34.20/7.53/0.96
couple	0.2	9.00/0.86/0.99	31.20/2.66/0.99	18.40/2.30/0.99
	0.4	6.20/0.91/0.98	32.60/4.08/0.98	27.60/5.07/0.98
	0.6	5.00/1.03/0.95	40.20/6.75/0.95	32.60/7.18/0.95
crowd	0.2	7.60/0.76/1.00	15.60/1.42/1.00	21.40/2.55/1.00
	0.4	6.00/0.85/0.99	31.20/3.89/0.99	21.40/3.99/0.99
	0.6	7.40/1.51/0.97	44.20/7.37/0.97	36.80/8.28/0.97
finger	0.2	21.80/0.36/0.94	22.80/0.38/0.94	12.20/0.22/0.94
	0.4	25.80/0.63/0.85	35.60/0.88/0.85	12.40/0.33/0.84
	0.6	23.80/0.68/0.71	39.20/1.06/0.71	9.00/0.27/0.69
girlface	0.2	15.40/1.61/0.99	16.60/1.56/0.99	12.40/1.39/0.99
	0.4	25.20/3.58/0.99	28.40/3.68/0.99	17.60/2.96/0.99
	0.6	51.00/9.73/0.97	38.80/6.66/0.97	26.20/5.95/0.97
houses	0.2	73.00/6.24/0.99	33.80/2.98/0.99	10.40/1.10/0.98
	0.4	147.60/17.96/0.96	47.80/5.95/0.96	53.80/9.34/0.96
	0.6	18.00/3.40/0.91	59.40/10.59/0.91	45.40/10.10/0.90
kiel	0.2	14.20/1.33/0.98	26.80/2.40/0.98	16.40/2.15/0.98
	0.4	9.00/1.35/0.95	46.80/6.21/0.95	27.20/5.45/0.95
	0.6	7.00/1.57/0.91	43.00/8.26/0.91	44.40/11.19/0.91

Contrinued on next page

Name	Noise	IRHCGP	IPDY	JHCGPM
		$NumI/RunT/SSIM$	$NumI/RunT/SSIM$	$NumI/RunT/SSIM$
lighthouse	0.2	19.80/1.94/0.99	23.20/2.16/0.99	5.40/0.64/0.98
	0.4	9.00/1.32/0.96	47.80/6.41/0.96	36.20/7.34/0.96
	0.6	6.80/1.47/0.91	47.60/8.89/0.91	60.80/14.83/0.91
lungs	0.2	6.20/0.46/1.00	10.20/0.76/1.00	11.20/0.84/1.00
	0.4	15.40/1.57/1.00	16.20/1.53/1.00	15.80/1.89/1.00
	0.6	26.20/2.80/0.99	20.80/2.13/0.99	17.80/2.10/0.99
man	0.2	28.20/13.46/1.00	20.40/8.90/1.00	7.00/3.58/1.00
	0.4	5.00/3.88/0.99	26.00/17.39/0.99	19.40/17.00/0.99
	0.6	6.00/5.52/0.98	40.80/29.18/0.98	27.20/25.00/0.98
pepper	0.2	6.80/0.66/0.99	41.00/3.50/0.99	12.40/1.41/0.99
	0.4	6.20/0.92/0.98	41.80/5.11/0.98	10.80/1.88/0.98
	0.6	86.20/16.05/0.97	59.80/9.89/0.97	20.20/4.53/0.97
sailboat	0.2	8.00/0.78/0.99	32.60/2.90/0.99	15.40/1.83/0.99
	0.4	6.00/0.89/0.98	33.40/4.23/0.98	33.80/6.19/0.98
	0.6	5.00/1.21/0.95	52.80/10.22/0.95	22.40/5.82/0.95
tank	0.2	7.00/0.82/0.99	17.80/1.90/0.99	17.60/2.16/0.99
	0.4	4.00/0.73/0.97	14.40/2.18/0.97	17.60/3.37/0.97
	0.6	38.40/7.81/0.94	28.20/5.11/0.94	19.80/4.56/0.94
tank2	0.2	5.60/0.59/0.99	14.20/1.39/0.99	7.00/0.77/0.99
	0.4	5.00/0.78/0.97	15.20/1.99/0.97	21.80/3.81/0.97
	0.6	7.00/1.72/0.94	25.00/5.17/0.94	20.60/5.40/0.94
tiffany	0.2	6.00/0.70/0.99	21.40/2.19/0.99	17.20/2.11/0.99
	0.4	5.00/0.85/0.98	33.60/4.59/0.98	19.60/3.81/0.98
	0.6	6.00/1.54/0.95	49.20/9.91/0.95	28.80/7.54/0.95
truck	0.2	5.60/0.65/0.99	18.00/1.82/0.99	9.60/1.21/0.99
	0.4	7.00/1.16/0.98	28.20/4.19/0.98	18.80/3.76/0.98
	0.6	40.60/7.75/0.95	26.60/4.57/0.95	27.40/5.95/0.95
trucks	0.2	7.00/0.69/0.99	15.40/1.41/0.99	18.60/2.19/0.99
	0.4	6.00/0.86/0.97	20.60/2.63/0.97	25.00/4.52/0.97
	0.6	5.00/1.03/0.94	25.20/4.35/0.94	21.40/4.69/0.94
zelda	0.2	7.60/0.79/1.00	14.40/1.35/1.00	12.60/1.40/1.00
	0.4	19.00/2.73/0.99	25.40/3.25/0.99	20.80/3.68/0.99
	0.6	42.00/7.93/0.98	26.40/4.52/0.98	24.20/5.32/0.98

Figure 3. From left to right: sailboat image with 20%/40%/60% impulse noise and image restoration from IRHCGP, IPDY, and JHCGPM algorithms.

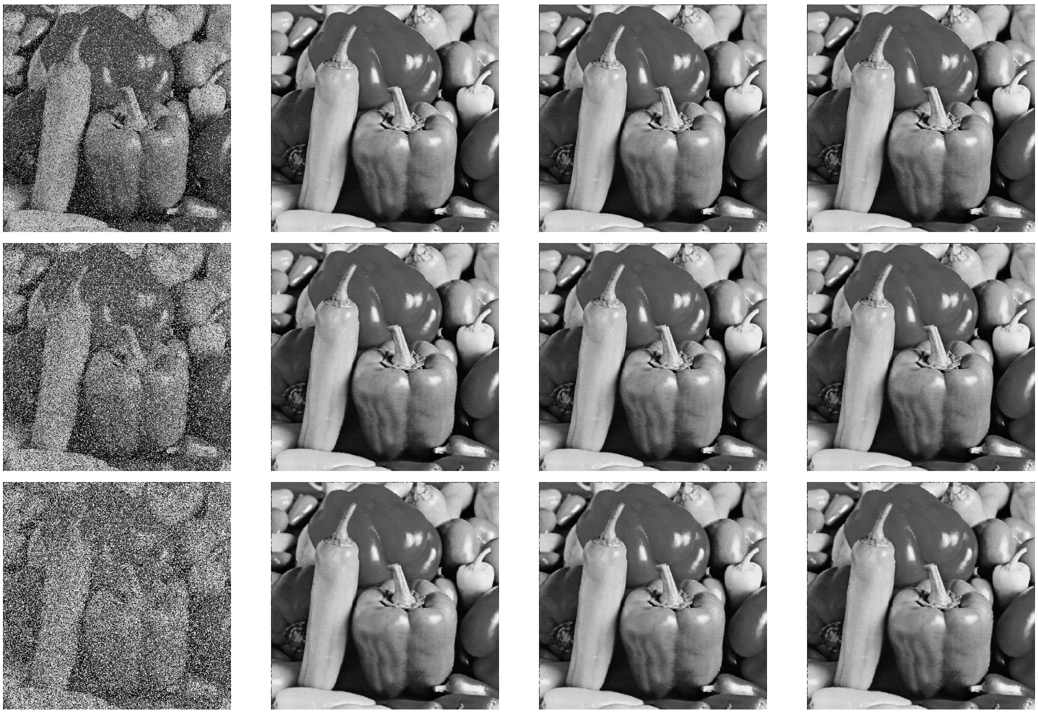

Figure 4. From left to right: pepper image with 20%/40%/60% impulse noise and image restoration from IRHCGP, IPDY, and JHCGPM algorithms.

6. Conclusions

In this paper, we introduce an IRHCGP method for solving constrained nonlinear equations. The core innovation of the proposed method lies in the construction of a hybrid search direction that integrates classical conjugate parameters with projection-based and inertial-relaxation strategies. This hybrid direction is shown to satisfy both the sufficient descent condition and the trust region condition, which are critical for ensuring global convergence. Theoretical analysis is conducted under relatively mild assumptions, establishing the global convergence of the proposed method without requiring stringent conditions often assumed in prior works. To validate the effectiveness of the proposed method, extensive numerical experiments are performed on two categories of problems: (i) large-scale constrained nonlinear systems, and (ii) impulse noise image restoration applications. The experimental results demonstrate that the proposed method is effective and promising when compared with the existing methods.

Author contributions

Dandan Li: Conceptualization, Investigation, Writing–original draft; Songhua Wang: Funding acquisition, Investigation; Jiaqi Wu: Conceptualization, Investigation, Writing–review and editing. All authors have read and approved the final version of the manuscript for publication.

Use of Generative-AI tools declaration

The authors declare they have not used Artificial Intelligence (AI) tools in the creation of this article.

Acknowledgments

This research was funded by the Natural Science Foundation in Guangxi Province (No. 2024GXNSFAA010478).

Conflict of interest

The authors declare that there are no conflicts of interest regarding the publication of this paper.

References

1. C. Byrne, A unified treatment of some iterative algorithms in signal processing and image reconstruction, *Inverse Probl.*, **20** (2003), 103. http://doi.org/10.1088/0266-5611/20/1/006
2. D. Li, S. Wang, Y. Li, J. Wu, A modified SGP method with two alternative spectral parameters for constrained nonlinear equations with a compressive sensing application, *J. Comput. Appl. Math.*, **463** (2025), 116503. https://doi.org/10.1016/j.cam.2025.116503
3. S. Boyd, N. Parikh, E. Chu, B. Peleato, J. Eckstein, Distributed optimization and statistical learning via the alternating direction method of multipliers, *Found. Trends Mach. Learn.*, **3** (2011), 1–122. https://doi.org/10.1561/2200000016

4. R. Diaz, J. Cervantes, R. Salcedo, M. Perez, Analysis of electrical power systems with Newton-type accelerated numerical methods, *SSRG Int. J. Elect. Electron. Eng.*, **10** (2023), 148–157. https://doi.org/10.14445/23488379/IJEEE-V10I11P114

5. N. Iusem, V. Solodov, Newton-type methods with generalized distances for constrained optimization, *Optimization*, **41** (1997), 257–278. https://doi.org/10.1080/02331939708844339

6. Y. Zhao, D. Li, Monotonicity of fixed point and normal mappings associated with variational inequality and its application, *SIAM J. Optim.*, **11** (2001), 962–973. https://doi.org/10.1137/S1052623499357957

7. D. Li, S. Wang, Y. Xia, X. Ma, Convergence analysis of a three-term extended RMIL CGP-based algorithm for constrained nonlinear equations and image denoising applications, *Electron. Res. Arch.*, **33** (2025), 3584–3612. https://doi.org/10.3934/era.2025160

8. O. Abu Arqub, Numerical simulation of time-fractional partial differential equations arising in fluid flows via reproducing Kernel method, *Int. J. Numer. Meth. Heat Fluid Flow*, **30** (2020), 4711–4733. https://doi.org/10.1108/HFF-10-2017-0394

9. H. Li, Projected Newton method for large-scale Bayesian linear inverse problems, *SIAM J. Optim.*, **35** (2025), 1439–1468. https://doi.org/10.1137/24M1645838

10. A. Izmailov, M. Solodov, On local behavior of Newton-type methods near critical solutions of constrained equations, *J. Optim. Theory Appl.*, **203** (2024), 1103–1126. https://doi.org/10.1007/s10957-023-02367-1

11. L. Qi, X. Tong, D. Li, Active-set projected trust region algorithm for box constrained nonsmooth equations, *J. Optim. Theory Appl.*, **120** (2004), 601–625. https://doi.org/10.1023/B:JOTA.0000025712.43243.eb

12. L. Qi, Z. Wei, G. Yuan, An active-set projected trust-region algorithm with limited memory BFGS technique for box-constrained nonsmooth equations, *Optimization*, **62** (2013), 857–878. https://doi.org/10.1080/02331934.2011.603321

13. D. Li, S. Wang, Y. Li, J. Wu, A convergence analysis of hybrid gradient projection algorithm for constrained nonlinear equations with applications in compressed sensing, *Numer. Algor.*, **95** (2024), 1325–1345. https://doi.org/10.1007/s11075-023-01610-0

14. D. Li, Y. Li, S. Wang, A family of projection-based spectral conjugate gradient algorithm for constrained monotone nonlinear equations with application, *Int. J. Comput. Meth.*, **22** (2025), 2450085. https://doi.org/10.1142/S0219876224500853

15. P. Liu, X. Wu, H. Shao, Y. Zhang, S. Cao, Three adaptive hybrid derivative-free projection methods for constrained monotone nonlinear equations and their applications, *Numer. Linear Algebra Appl.*, **30** (2023), e2471. https://doi.org/10.1002/nla.2471

16. W. Kumam, J. Vigo-Aguiar, P. Kumam, Projection method for solving large-scale system of nonlinear equations, *Nonlinear Convex Anal. Optim.*, **2** (2023), 93–112. https://doi.org/10.58715/ncao.2023.2.5

17. Z. Zhu, D. Zhang, S. Wang, Two modified DY conjugate gradient methods for unconstrained optimization problems, *Appl. Math. Comput.*, **373** (2020), 125004. https://doi.org/10.1016/j.amc.2019.125004

18. Y. Ou, L. Li, A unified convergence analysis of the derivative-free projection-based method for constrained nonlinear monotone equations, *Numer. Algor.*, **93** (2023), 1639–1660. https://doi.org/10.1007/s11075-022-01483-9

19. X. Jiang, Y. Deng, J. Jian, A memoryless Broyden-Fletcher-Goldfarb-Shanno-type projection method with self-adjusting line search for convexly constrained monotone equations and its applications, *Numer. Algor.*, 2026. https://doi.org/10.1007/s11075-026-02340-9

20. F. Alvarez, On the minimizing property of a second order dissipative system in Hilbert spaces, *SIAM J. Control Optim.* **38** (2000), 1102–1119. https://doi.org/10.1137/S0363012998335802

21. P. Liu, J. Li, H. Shao, T. Wu, An accelerated derivative-free memoryless Davidon-Fletcher-Powell method and its iteration-complexity analysis, *J. Sci. Comput.* **105** (2025), 43. https://doi.org/10.1007/s10915-025-03071-0

22. P. Liu, L. Li, F. Shao, K. Li, An accelerated hybrid three-term derivative-free projection method with applications, *Optim. Lett.* **20** (2026), 841–872. https://doi.org/10.1007/s11590-025-02262-w

23. S. Aji, P. Kumam, A. Awwal, M. Yahay, A. Bakoji, A new inertial-based method for solving pseudomonotone operator equations with application, *Comput. Appl. Math.*, **42** (2023), 1. https://doi.org/10.1007/s40314-022-02135-3

24. P. Liu, L. Li, H. Shao, M. Liu, J. Fan, An inertial-type CG projection method with restart for pseudo-monotone costs with application to traffic assignment, *Netw. Spat. Econ.*, **25** (2025), 147–172. https://doi.org/10.1007/s11067-024-09653-z

25. H. Zheng, J. Li, P. Liu, X. Rong, An inertial Fletcher-Reeves-type conjugate gradient projection-based method and its spectral extension for constrained nonlinear equations, *J. Appl. Math. Comput.*, **70** (2024), 2427–2452. https://doi.org/10.1007/s12190-024-02062-y

26. P. Liu, L. Li, H. Shao, B. Zhang, An accelerated spectral CG-type projection method with restart strategy for nonlinear monotone equations and applications in compressed sensing, *Numer. Linear Algebra Appl.*, **32** (2025), e70035. https://doi.org/10.1002/nla.70035

27. Y. Zhuo, X. Wu, J. Zhou, An inertial three-term hybrid CG-based projection method for constrained nonlinear pseudo-monotone equations with applications, *Numer. Algebra Contr. Optim.*, **14** (2024), 581–600. https://doi.org/10.3934/naco.2023009

28. N. Andrei, Another hybrid conjugate gradient algorithmfor unconstrained optimization, *Numer. Algor.*, **47** (2008), 143–156. https://doi.org/10.1007/s11075-007-9152-9

29. N. Andrei, Hybrid conjugate gradient algorithm for unconstrained optimization, *J. Optim. Theory Appl.*, **141** (2009), 249–264. https://doi.org/10.1007/s10957-008-9505-0

30. Z. Wei, H. Huang, Y. Tao, A modified Hestenes-Stiefel conjugate gradient method and its convergence, *J. Math. Res. Expo.*, **30** (2010), 297–308.

31. D. Li, Y. Li, S. Wang, Solving constrained nonlinear equations with an inertial-based hybrid three-term CGP algorithm: application to image denoising, *J. Appl. Math. Comput.*, **71** (2025), 1109–1136. https://doi.org/10.1007/s12190-025-02525-w

32. A. Ibrahim, P. Kumam, A. Abubakar, J. Abubakar, A method with inertial extrapolation step for convex constrained monotone equations, *J. Inequal. Appl.*, **2021** (2021), 189. https://doi.org/10.1186/s13660-021-02719-3

33. X. Jiang, Z. Huang, An accelerated relaxed-inertial strategy based CGP algorithm with restart technique for constrained nonlinear pseudo-monotone equations to image de-blurring problems, *J. Comput. Appl. Math.*, **447** (2024), 115887. https://doi.org/10.1016/j.cam.2024.115887

34. J. Yin, J. Jian, X. Jiang, X. Wu, A family of inertial-relaxed DFPM-based algorithms for solving large-scale monotone nonlinear equations with application to sparse signal restoration, *J. Comput. Appl. Math.*, **419** (2023), 114674. https://doi.org/10.1016/j.cam.2022.114674

35. J. Sabi'u, S. Sirisubtawee, An inertial Dai-Liao conjugate method for convex constrained monotone equations that avoids the direction of maximum magnification, *J. Appl. Math. Comput.*, **70** (2024), 4319–4351. https://doi.org/10.1007/s12190-024-02123-2

36. E. Dolan, J. Moré, Benchmarking optimization software with performance profiles, *Math. Program.*, **91** (2002), 201–213. https://doi.org/10.1007/s101070100263

37. R. Chan, C. Ho, M. Nikolova, Salt-and-pepper noise removal by median-type noise detectors and detail-preserving regularization, *IEEE Trans. Image Process.*, **14** (2005), 1479–1485. https://doi.org/10.1109/TIP.2005.852196

AIMS Press